Exhumation history and timing of supergene copper mineralisation in an arid climate: New thermochronological data from the Centinela District, Atacama, Chile

Article *in* Terra Nova · November 2017

DOI: 10.1111/ter.12311

11 authors, including:

Caroline Sanchez
Géosciences Environnement Toulouse - Observatoire Midi-Pyrénées

Stephanie Brichau
Institute of Research for Development

Sebastien Carretier
Institute of Research for Development

Thomas Bissig
Goldcorp

MISS CAROLINE SANCHEZ (Orcid ID : 0000-0002-9526-4759)

Article type : Paper

Received date: 13-Dec-2016
Revised version received date: 27-Sep-2017
Accepted date: 01-Oct-2017

Exhumation history and timing of supergene copper mineralization in an arid climate: new thermochronological data from the Centinela District, Atacama, Chile

Correspondence details:
Miss Caroline Sanchez
Depto. Ciencias Geológicas
Universidad Catolica del Norte
Avenida Angamos 0610
Antofagasta
Chile

Tel: +56-55-2355970
E-mail: csanchez@get.obs-mip.fr

Caroline Sanchez[1, 2], Stéphanie Brichau[2], Rodrigo Riquelme[1], Sébastien Carretier[2], Thomas Bissig[4], Cristopher Lopez[1], Constantino Mpodozis[3], Eduardo Campos[1], Vincent Regard[2], Gérard Hérail[2], Carlos Marquardt[5]

[1]*Depto. Ciencias Geológicas, Universidad Católica del Norte, Avenida Angamos 0610, Antofagasta, Chile.*

This article has been accepted for publication and undergone full peer review but has not been through the copyediting, typesetting, pagination and proofreading process, which may lead to differences between this version and the Version of Record. Please cite this article as doi: 10.1111/ter.12311

[2]*Géosciences Environnement Toulouse (GET), Université de Toulouse, UPS, CNRS, IRD, CNES, Toulouse, France.*

[3]*Antofagasta Minerals S.A., Avenida Apoquindo. 4001, piso 18, Las Condes, Santiago, Chile.*

[4]*Mineral Deposit Research Unit, Department of Earth, Ocean and Atmospheric Sciences, University of British Columbia, Vancouver, BC, Canada V6T 1Z4*

[5]*Departamento de Ingeniería en Minería, Pontificia Universidad Católica de Chile, Santiago, Chile*

ABSTRACT:

Supergene copper mineralization processes occur during the unroofing of porphyry copper deposits. However, the geomorphological stage during which the main mineralization occurs is still under debate. Here, we present 24 new thermochronological data from Cenozoic intrusives and compare them with the evolution of supergene mineralization from the Centinela Mining District in the Atacama Desert. Our results indicate a two-step cooling path: a rapid Late Eocene exhumation followed by a slow denudation. Previously published supergene mineralization ages cluster after the main Upper Oligocene exhumation period. Ours is the first study that establishes the relationship between exhumation and supergene processes on the scale of a single mining district. It confirms that supergene copper mineralization took place during pediplanation, likely a required condition for efficient supergene copper mineralization under arid climatic conditions, in contrast to wet tropical environments where supergene copper mineralization occurs during rapid relief growth but has limited preservation potential.

INTRODUCTION

Porphyry copper deposits are genetically linked to the emplacement of shallow intrusions (< 5km deep: Richards, 2011; Wilkinson, 2013), on which hypogene sulfide mineralization precipitates from magmatic–hydrothermal fluids (Seedorff *et al*., 2005), but copper grades may increase substantially after exhumation when sulfides are exposed to oxidation and leaching. Leached copper may precipitate as either copper oxides or secondary enriched sulfides depending on whether precipitation occurs above or below the water table (Chavez, 2000; Sillitoe, 2005).

Climatic and geomorphologic conditions favouring supergene copper mineralization (SCM) are still a matter of debate (Reich and Vasconcelos, 2015). SCM is thought to be particularly efficient under semi-arid climates, where moderate precipitation provides high water-to-rock ratios and denudation is limited, preserving the weathering profile (e.g. Clark *et al*., 1990, Vasconcelos, 1999; Hartley and Rice, 2005). However, rare SCM examples have been documented in tropical rapidly uplifted environments (Bamford, 1972; Braxton *et al*., 2011).

SCM requires an equilibrium between denudation and water-table descent rates, which can be encountered at different stages of the landscape evolution in response to surface uplift (Mortimer, 1973; Alpers and Brimhall, 1988; Bouzari and Clark, 2002). During this cycle, illustrated in three stages, the erosion rate follows a “humped” curve (e.g. Kooi and Beaumont, 1996; Fig.1).

Previous studies have proposed that SCM may occur: 1) during the increasing relief, denudation and river incision phase (Fig.1A) (Sillitoe and Perelló, 2005; Bissig and Riquelme, 2009; 2010); 2) during the maximum hillslope angle and denudation rate period (Fig.1B; Braxton *et al*., 2009); or 3) during landscape pediplanation (Fig.1C) when denudation and slopes decrease (Mortimer, 1973; Clark *et al*., 1990; Bouzari and Clark, 2002; Quang *et al*., 2005).

In the Atacama Desert, the SCM development in numerous Cenozoic porphyry copper deposits has been placed within the physiographic context of Upper Oligocene–Lower Miocene erosional pediments (e.g., Mortimer, 1973; Alpers and Brimhall, 1988). The role of pediment formation in SCM remains unclear. Distinct supergene episodes have been correlated with brief intervals of uplift and pediment incision (e.g. Bouzari and Clark, 2002; Quang *et al*., 2005; Bissig and Riquelme, 2010), whereas Sillitoe (2005) argued that thick SCM develop during major surface uplift events, implying that pediplanation is not required for efficient supergene formation. Conversely, Hartley and Rice (2005) proposed that the influence of regional pediplain formation on SCM is not well established, mainly due to the lack of landform ages. To tackle this issue, we focused on the Centinela District (CD) in northern Chile (Fig.2A,B), where most of the world-class SCMs are hosted beneath pediplains (Sergestrom, 1963; Mortimer, 1973).

We performed a thermochronological study to identify when in the geomorphological cycle SCM took place. Four zircon U–Pb, six apatite fission-track (AFT) and ten apatite helium (AHe) ages were obtained and compared with published supergene minerals' $^{40}Ar/^{39}Ar$ and K–Ar ages (see supplementary data; Sillitoe and McKee, 1996; Perelló *et al*., 2010; Riquelme *et al.*, accepted). In northern Chile, low-temperature thermochronological studies have been conducted on specific porphyries (McInnes *et al*., 1999; Campos *et al*., 2009; Maksaev *et al*., 2010) to constrain their cooling/exhumation history, yet none has been performed at a mining-district scale. The CD is a key area including both exhumed porphyries and SCMs. Our samples were taken from both mineralized and non-Cu-mineralized intrusions. Their denudation is recorded in the mid-Eocene to Upper Miocene gravel deposits that constitute the CD sedimentary cover (Mora *et al*., 2004, Riquelme *et al*., accepted).

GEOLOGICAL BACKGROUND

The CD is located 60 km south of Calama (Fig.2B) on the western limb of the Precordillera. The district includes outcrops of Palaeozoic basement, Mesozoic volcanic and sedimentary rocks, and Palaeocene volcanic rocks (Mpodozis and Cornejo, 2012; Fig.2C). These rocks are intruded by Lower Cretaceous–Upper Eocene diorites and rhyolitic and dacitic porphyry intrusions (Mpodozis and Cornejo, 2012; Marinovic and Garcia, 1999).

Two regional-scale tectonic phases affected the CD during the Cenozoic. The first phase, characterized by crustal shortening and labelled K–T, occurred at ~60 Ma and was accompanied by Palaeocene intrusions (Cornejo *et al.*, 2003; Mpodozis and Cornejo, 2012), whereas porphyry-Cu mineralization is related to intrusions emplaced between 45 and 41 Ma, during the Incaic orogenic phase (Perelló *et al*., 2004; Mpodozis *et al*., 2009). The Incaic phase activated the 800 km long N-trending transpressive Domeyko Fault System in the Precordillera, upthrowing porphyry-Cu intrusions to the west and allowing the formation of structurally controlled basins (Fig. 2C) to the east (Mpodozis *et al.*, 1993; Amilibia *et al*., 2008, Mpodozis and Cornejo, 2012). In the CD, Precordilleran erosion and denudation in response to the Incaic phase resulted in the deposition of up to ~ 800 metres of mid-late Eocene to Late Miocene gravel and sand deposits with scarce interbedded volcanic and evaporitic layers (Mora *et al*., 2004; Riquelme et al., accepted).

In the Atacama Desert, most supergene mineralization ages range from ~25 to 13 Ma (Sillitoe and Mckee, 1996; Arancibia *et al*., 2006; Reich *et al*., 2009; Bissig and Riquelme, 2010; Perello *et al.*, 2010; Riquelme *et al.*, accepted). In northern Chile, supergene mineralization ages are generally younger than exhumation ages (Arancibia *et al*., 2006, Maksaev and Zentilli, 1999) but precise SCM onset remains difficult to date. In the CD, supergene alunite and jarosite ^{40}Ar–^{39}Ar and K–Ar ages range from 25 to 13 Ma, matching previously obtained SCM ages and the age of hyperaridity onset in the area (Alpers and Brimhall, 1988; Dunai *et al.*, 2005).

METHODS

Ten Palaeogene–Upper Eocene equigranular granodioritic and sub-volcanic dacitic porphyry intrusives were sampled in the CD (Table 1). Apatite and zircon were extracted from the samples using conventional mineral separation techniques at the Geosciences Environnement Toulouse (GET) laboratory (France).

AFT analyses were jointly carried out at GET and Universidad de Chile, while irradiations were performed in the Chilean CCHEN nuclear reactor; AHe analyses were performed at the Geosciences Montpellier laboratory, France, and zircon U–Pb dating was performed at Birbeck College, London, UK. Detailed laboratory procedures are described in Witt *et al*. (2012), Eude *et al*. (2015) and Wu *et al*. (2016). Results are summarized in Table 1.

To extract thermal histories from the six samples providing both AFT and AHe ages, we used Ketcham's HeFTy modelling package (Ketcham, 2005). For visual representation, we extracted two cooling histories representing good paths and the average best fit for each sample from Lower Palaeogene granodiorite and Middle Eocene dacitic intrusions (Fig.3; see details in data repository section 2).

RESULTS

Our new AFT and AHe ages provide evidence of two intrusive cooling histories. Lower Palaeocene granodiorites display zircon U–Pb ages of 64.4 ± 1.4 Ma and 64.9 ± 1.2 Ma, AFT ages from 46.1 ± 4.8 Ma to 41.1 ± 3.1 Ma, and AHe ages ranging from 45.0 ± 2.3 Ma to 22.4 ± 1.1 Ma (Fig.3). Mid-Eocene dacitic samples yielded zircon U–Pb ages from 42.7 ± 1.1 Ma to 39.7 ± 1.1 Ma, AFT ages of 46.1 ± 4.8 Ma to 41.1 ± 3.1 Ma, and AHe ages between 40.6 ±3.3 Ma and 37.9 ± 5.2 Ma. Modelling of these data suggest rapid cooling between ~60 and 35 Ma for the granodiorites and even faster cooling between ~40 and 30 Ma for the dacitic samples, followed, in both cases, by minor cooling (Fig.3).

DISCUSSION

New constraints on emplacement depth

To estimate Lower Palaeocene and middle Eocene porphyry copper emplacement depths, we divided the AFT (110°C, Gunnel *et al.*, 2000) and AHe (75°C, Farley, 2002) closure temperatures by a geothermal gradient estimated for the area at ~30–25°C/km (Morgan *et al.*, 1984). This suggests closure-temperature depths of 4.5–3.7 km for the AFT chronometer and 2.5–3 km for the AHe system. Lower Palaeocene granodiorite displays zircon U–Pb emplacement ages ~20 My older than the AFT ages, suggesting a minimum emplacement depth of 4.5–3.7 km. Eocene dacitic samples have emplacement ages that are similar to AFT ages but ~10 Ma older than the AHe ages, suggesting an emplacement depth between 4.5–3.7 km and 2.5–3 km. This difference is consistent with sample petrographic characteristics (Perello *et al.*, 2004). This suggests that Lower Palaeocene granodiorite exhumation started before and from a greater depth than the exhumation of the Eocene dacitic bodies.

Tectonic implications

The low-temperature thermochronology results indicate a protracted cooling phase in all samples. Lower Palaeocene intrusions experienced a rapid cooling from ~65 Ma to ~30 Ma, which may have been initiated by a rock exhumation episode during the K–T tectonic phase (Cornejo *et al.*, 1993; Mpodozis and Cornejo, 2012). On the other hand, Eocene dacitic intrusions have similar zircon U–Pb and AFT ages, and display a rapid cooling from 40 to

~30 Ma. This fast cooling is consistent with emplacement during the Incaic tectonic phase (Steinmann *et al.*, 1929; Noble et al., 1979; Charrier *et al.*, 2007). The duration of this major tectonic phase is the subject of debate. Hammerschmit (1992) and Tomlinson and Blanco (1997a) considered it a short tectonic contractile event at about 42 Ma, whereas Maksaev and Zentilli (1999) and Jaillard *et al.* (2000) proposed a duration from ~55 to ~30 Ma. Our results support the latter scenario.

After the Incaic tectonic phase, Eocene and Palaeocene intrusions exhibit a slow cooling path suggesting only minor exhumation not exceeding 2.5 km since the Early Oligocene. This can be related to the generalized landscape pediplanation reported for the Atacama Desert during Oligocene–Miocene time (Mortimer 1973; Isaack, 1988; Riquelme *et al.*, 2007; Evenstar *et al.*, 2009).

Relationship between exhumation and supergene mineralization

The relationship between exhumation and the onset of SCM has previously been studied at the El Salvador deposit, 400 km south of CD (Mote *et al.*, 2001; Bissig and Riquelme, 2010). There, supergene mineralization initiated at ~35 Ma, some 6 Ma after hypogene mineralization, suggesting rapid exhumation. However, the exhumation history of the porphyries is not constrained by thermochronology, and it is not known whether supergene mineralization occurred during relief growth or pediplanation. Similarly, at La Escondida mine, 200 km south of CD, Alpers and Brimhall (1988) found that hypogene hydrothermal alteration occurred around ~34–31 Ma, while SCM was active at ~18–14 Ma. Using mass balance calculations (Brimhall et al., 1995) and taking the unmineralized lithocap as a reference surface, Alpers and Brimhall (1988) discussed scenarios linking denudation history and SCM. However, uncertainties about the timing of the onset of SCM combined with a lack of exhumation data prevented them from determining whether supergene mineralization occurred after a rapid denudation period or during a constant, slow denudation phase.

This study provides new constraints on the relationship between SCM and pediplanation. Specifically, the difference between the timing of exhumation and the SCM ages (Fig.3) indicates that supergene mineralization (25–13 Ma data from Sillitoe and Mckee, 1996, Perello *et al.*, 2004 and Riquelme *et al,* accepted) occurred between 5 and 15 Ma after the end of rapid exhumation of the porphyry copper mineralization (~40–30 Ma). The relative tectonic quiescence inferred from the low exhumation rates after 30 Ma (Fig. 3) suggests that the district landscape was already in the pediplanation stage when supergene mineralization occurred (Fig. 1C). For other areas of the Atacama Desert, Arancibia *et al.* (2006) proposed that older SCM may have been eroded away. If so, SCM could have formed during the main unroofing period associated with the Incaic deformation and not only during pediplanation. However, for the CD we regard this as unlikely since no evidence of SCM detrital clasts older than ~25 Ma has been found in Centinela Basin sediments (Riquelme *et al.*, accepted). Thus, low erosion rates and low relief are conducive not only to preservation but also to supergene Cu mineralization in arid climates.

Climatic and tectonic controls on SCM

Wetter periods during the Oligo-Miocene may have controlled SCM periods in northern Chile's planar landscapes (Alpers and Brimhall, 1988; Sillitoe and McKee, 1996; Reich *et al.*, 2009) as well as in other climatic zones (Feng and Vasconcelos, 2007; Vasconcelos et al., 2015).

The apparent difficulty of developing significant SCM during rapid exhumation may not apply to humid environments where extensive SCM during rapid exhumation has been documented (Bamford 1972; Braxton et al., 2009; 2012). Transport-reactive models may help to clarify the differences between northern Chile and tropical examples (Mathur and Fantle, 2015). Under arid climates, primary copper dissolution may be limited by slow diffusion of copper species into the interstitial fluid (Lebedeva and Brantley, 2010). The weathered-layer thickening rate may be too slow to outpace the denudation rate during the main exhumation period. Even if there are more humid periods, the runoff excess may foster erosion on steep slopes and prevent the weathered layer from thickening. Once the slopes are gentle during pediplanation, the weathering profile can thicken. More humid periods will then favour groundwater infiltration, with a limited impact on erosion, favoring leaching as well as SCM at depth (Palacios *et al.*, 2011). In humid environments, sulfide dissolution may be controlled more by the groundwater velocity and thus may be rapid (Maher, 2010). While leaching is more efficient, chemical saturation requires in turn great groundwater penetration depths (Mathur and Fantle, 2015), limiting the SCM in stable landscapes (Carajás Mountains, Brazil – Vasconcelos et al., 2015). Nevertheless, if the protolith is exhuming fast (Boyongan and Bayugo deposits), the vertical supply of primary copper sulfides allows the Cu concentration in the descending groundwater to increase, so SCM saturation and precipitation may occur in the vadose (Cu oxide minerals, Boyongan and Bayugo) or saturated (enriched sulfides, Ok Tedi) zone. Although other factors locally control the SCM (pyrite content, bacteria, initial rock porosity etc; Braxton et al., 2009), such a process may explain the difference in optimum exhumation–climate combinations between the humid cases and the CD.

The time required to form a mature supergene profile most likely depends on the balance between exhumation and precipitation rates. In the case of the Ok Tedi, Boyongan and Bayugo districts, high exhumation rates are balanced by high precipitation rates (2,000–4,000 mm/a) allowing a mature supergene profile to form within a few hundreds of thousands of years. In contrast, when primary ore is subjected to low exhumation and precipitation rates, the formation of mature supergene profiles may require more than 10 Ma, as is suggested by the supergene mineralization ages of the CD.

CONCLUSION

Our data from the CD intrusions suggest that two important tectonic phases can be identified from the intrusive paths: the K–T tectonic phase (Cretaceous–Palaeogene limits) followed by the Incaic deformation (mid-Eocene and Early Oligocene). From the Incaic phase to the present-day, slow cooling paths can be related to landscape pediplanation. Our results provide quantitative support to previous interpretations suggesting that low denudation rates and low relief are favourable for SCM in arid environments.

ACKNOWLEDGMENTS

We acknowledge Fondecyt project no. 1121049, REDES funding no.140153, Copedim, IRD for funding this research and Conicyt, Universidad Católica del Norte and Université Paul Sabatier for granting this PhD work. Thank you to Marcelo Farias for access to the fission track laboratory in the Universidad de Chile. We are also grateful for logistical support from Antofagasta Minerals (AMSA) in the field. Finally, we thank Patrick Monié and Michael Bonno from the Geoscience Laboratoire in Montpellier and Andrew Carter from Birkbeck College for their analytical help.

REFERENCES

Alpers, C. N., and Brimhall, G. H. 1988. Middle Miocene climatic change in the Atacama Desert, northern Chile: Evidence from supergene mineralization at La Escondida. *Geological Society of America Bulletin*, **100**, 1640–1656.

Amilibia, A., Sàbat, F., McClay, K. R., Muñoz, J. A., Roca, E., and Chong, G. 2008. The role of inherited tectono-sedimentary architecture in the development of the central Andean mountain belt: Insights from the Cordillera de Domeyko. *Journal of Structural Geology*, **30**, 1520–1539.

Andriessen, P. A., and Reutter, K.-J. 1994. K-Ar and fission track mineral age determination of igneous rocks related to multiple magmatic arc systems along the 23 S latitude of Chile and NW Argentina. *Tectonics of the southern central Andes: structure and evolution of an active continental margin*, 141–154.

Arancibia, G., Matthews, S. J., and de Arce, C. P. 2006. K–Ar and 40Ar/39Ar geochronology of supergene processes in the Atacama Desert, Northern Chile: tectonic and climatic relations. *Journal of the Geological Society*, **163**, 107–118.

Bamford, R. W. 1972. The Mount Fubilan (Ok Tedi) Porphyry Copper Deposit, Territory of Papua and New Guinea. *Economic Geology*, **67**, 1019–1033.

Bissig, T., and Riquelme, R. 2009. Contrasting landscape evolution and development of supergene enrichment in the El Salvador porphyry Cu and Potrerillos-El Hueso Cu-Au districts, northern Chile. *Supergene Environments, Processes and Products (Titley S.; editor). Society of Economic Geologists Special Publication*, **14**, 59–68.

Bissig, T., and Riquelme, R. 2010. Andean uplift and climate evolution in the southern Atacama Desert deduced from geomorphology and supergene alunite-group minerals. *Earth and Planetary Science Letters*, **299**, 447–457.

Bouzari, F., and Clark, A. H. 2002. Anatomy, evolution, and metallogenic significance of the supergene orebody of the Cerro Colorado porphyry copper deposit, I Región, northern Chile. *Economic Geology*, **97**, 1701–1740.

Braun, J., Mercier, J., Guillocheau, F., and Robin, C. 2016. A simple model for regolith formation by chemical weathering. *Journal of Geophysical Research: Earth Surface*, **121**, 2140-2171.

Braxton, D., and Mathur, R. 2011. Exploration applications of copper isotopes in the supergene environment: A case study of the Bayugo porphyry copper-gold Deposit, southern Philippines. *Economic Geology*, **106**, 1447–1463.

Braxton, D. P., Cooke, D. R., Dunlap, J., Norman, M., Reiners, P., Stein, H., and Waters, P. 2012. From crucible to graben in 2.3 Ma: A high-resolution geochronological study of porphyry life cycles, Boyongan-Bayugo copper-gold deposits, Philippines. *Geology*, **40**, 471–474.

Braxton, D. P., Cooke, D. R., Ignacio, A. M., Rye, R. O., and Waters, P. J. 2009. Ultra-deep oxidation and exotic copper formation at the late Pliocene Boyongan and Bayugo porphyry copper-gold deposits, Surigao, Philippines: geology, mineralogy, paleoaltimetry, and their implications for geologic, physiographic, and tectonic controls. *Economic Geology*, **104**, 333–349.

Campos, E., Wijbrans, J., and Andriessen, P. A. 2009. New thermochronologic constraints on the evolution of the Zaldívar porphyry copper deposit, Northern Chile. *Mineralium Deposita*, **44**, 329.

Charrier, R., Pinto, L., and Rodríguez, M. P. 2007. Tectonostratigraphic evolution of the Andean Orogen in Chile. *The Geology of Chile*, 21–114.

Chávez Jr, W. X. 2000. Supergene oxidation of copper deposits: zoning and distribution of copper oxide minerals. *Soc. Econ. Geol. Newsl.*, **41**, 10–21.

Clark, A. H., Tosdal, R. M., Farrar, E., and Plazolles, A. 1990. Geomorphologic environment and age of supergene enrichment of the Cuajone, Quellaveco, and

Toquepala porphyry copper deposits, southeastern Peru. *Economic Geology*, **85**, 1604–1628.

Clark, A. H., Mayer, A. E. S., Mortimer, C., Sillitoe, R. H., Cooke, R. U., and Snelling, N. J. (1967). Implications of the isotopic ages of ignimbrite flows, southern Atacama Desert, Chile. *Nature*, **215**, 723-724.

Cornejo, P., Matthews, S., and Pérez de Arce, C. 2003. The "K-T" Compressive Deformation Event in Northern Chile (24-27°). *10^{o} Congreso Geológico Chileno, Concepción.*

Deckart, K., Clark, A. H., Cuadra, P., and Fanning, M. 2013. Refinement of the time-space evolution of the giant Mio-Pliocene Río Blanco-Los Bronces porphyry Cu–Mo cluster, Central Chile: new U–Pb (SHRIMP II) and Re–Os geochronology and 40Ar/39Ar thermochronology data. *Mineralium Deposita*, **48**, 57–79

Dunai, T. J., López, G. A. G., and Juez-Larré, J. 2005. Oligocene–Miocene age of aridity in the Atacama Desert revealed by exposure dating of erosion-sensitive landforms. *Geology*, **33**, 321-324.

Eude, A., Roddaz, M., Brichau, S., Brusset, S., Calderon, Y., Baby, P., and Soula, J.-C. 2015. Controls on timing of exhumation and deformation in the northern Peruvian eastern Andean wedge as inferred from low-temperature thermochronology and balanced cross section. *Tectonics*, **34**, 715–730.

Evenstar, L. A., Hartley, A. J., Stuart, F. M., Mather, A. E., Rice, C. M., and Chong, G. 2009. Multiphase development of the Atacama Planation Surface recorded by cosmogenic 3He exposure ages: Implications for uplift and Cenozoic climate change in western South America. *Geology*, **37**, 27–30.

Farley, K. A. 2002. (U-Th)/He dating: Techniques, calibrations, and applications. *Reviews in Mineralogy and Geochemistry*, **47**, 819–844.

Feng, Y.-X., and Vasconcelos, P. 2007. Chronology of Pleistocene weathering processes, southeast Queensland, Australia. *Earth and Planetary Science Letters*, **263**, 275–287.

Gunnell, Y. 2000. Apatite fission track thermochronology: an overview of its potential and limitations in geomorphology. *Basin Research*, **12**, 115–132.

Hammerschmidt, K., Döbel, R., and Friedrichsen, H. 1992. Implication of 40Ar39Ar dating of Early Tertiary volcanic rocks from the north-Chilean Precordillera. *Tectonophysics*, **202**, 55–81.

Hartley, A. J., and Rice, C. M. 2005. Controls on supergene enrichment of porphyry copper deposits in the Central Andes: a review and discussion. *Mineralium Deposita*, **40**, 515–525

Isacks, B. L. (1988). Uplift of the central Andean plateau and bending of the Bolivian orocline. *Journal of Geophysical Research: Solid Earth*, *93*(B4), 3211-3231.

Jaillard, E., Hérail, G., Monfret, T., Díaz-Martínez, E., Baby, P., Lavenu, A., and Dumont, J. F. 2000. Tectonic evolution of the Andes of Ecuador, Peru, Bolivia and northernmost Chile. *Tectonic Evolution of South America*, **31**, 481–559.

Jordan, T. E., Isacks, B., Ramos, V. A., and Allmendinger, R. W. 1983. Mountain building in the Central Andes. *Episodes*, **3**, 20–26.

Ketcham, R. A. 2005. HeFTy: Forward and inverse modeling thermochronometer systems. *Computational Tools for Low-Temperature Thermocronometer Interpretation. Mineralogical Society of America, Chantilly, VA.*

Kooi, H., and Beaumont, C. 1996. Large-scale geomorphology: Classical concepts reconciled and integrated with contemporary ideas via a surface processes model. *Journal of Geophysical Research: Solid Earth*, **101**, 3361–3386.

Lebedeva, M. I., Fletcher, R. C., and Brantley, S. L. 2010. A mathematical model for steady-state regolith production at constant erosion rate. *Earth Surface Processes and Landforms*, **35**, 508–524.

Maher, K. 2010. The dependence of chemical weathering rates on fluid residence time. *Earth and Planetary Science Letters,* **294**, 101–110.

Maksaev, V., Almonacid, T. A., Munizaga, F., Valencia, V., McWilliams, M., and Barra, F. 2010. Geochronological and thermochronological constraints on porphyry copper mineralization in the Domeyko alteration zone, northern Chile. *Andean Geology*, **37**.

Maksaev, V., and Zentilli, M. 1999. Fission track thermochronology of the Domeyko Cordillera, northern Chile: Implications for Andean tectonics and porphyry copper metallogenesis. *Exploration and Mining Geology*, **8**, 65–90.

Marinovic, N. and García, M., 1999. Hoja Pampa Unión, Región de Antofagasta. Escala 1:100.000, Servicio Nacional de Geología y Minería, Mapas Geológicos, N° 9, Santiago.

Mathur, R., and Fantle, M. S. 2015. Copper Isotopic Perspectives on Supergene Processes: Implications for the Global Cu Cycle. *Elements*, **11**, 323329.

McInnes, B. I., Farley, K. A., Sillitoe, R. H., and Kohn, B. P. 1999. Application of apatite (U-Th)/He thermochronometry to the determination of the sense and amount of vertical fault displacement at the Chuquicamata porphyry copper deposit, Chile. *Economic Geology,* **94**, 937–947.

Mora, R., Artal, J., Brockway, H., Martinez, E., and Muhr, R. 2004. El Tesoro exotic copper deposit, Antofagasta region, northern Chile. *Society of Economic Geologists, Special Publication*, **11**, 187–197.

Morgan, P. 1984. The thermal structure and thermal evolution of the continental lithosphere. *Physics and Chemistry of the Earth*, **15**, 107–193.

Mortimer, C. 1973. The Cenozoic history of the southern Atacama Desert, Chile. *Journal of the Geological Society*, **129**, 505–526.

Mote, T. I., Becker, T. A., Renne, P., and Brimhall, G. H. 2001. Chronology of exotic mineralization at El Salvador, Chile, by 40 Ar/39 Ar dating of copper wad and supergene alunite. *Economic Geology*, **96**, 351–366.

Mpodozis, C., Cembrano, J., and Mora, R. 2009. Deformación compresiva-oblicua polifásica y pórfidos cupríferos eocenos en el Sistema de Fallas de Domeyko: la región de Esperanza-Caracoles (Distrito Centinela), 12°Congreso Geológico Chileno *Santiago*, **22**.

Mpodozis, C., and Cornejo, P. 2012. Cenozoic tectonics and porphyry copper systems of the Chilean Andes. *Society of Economic Geologists Special Publication*, *16*, 329–360.

Mpodozis, C., Marinovic, N., and Smoje, I. 1993. Eocene left lateral strike slip faulting and clockwise block rotations in the Cordillera de Domeyko, west of Salar de Atacama, northern Chile. Géodynamique Andine: Symposium International II

Noble, D. C., McKee, E. H., and Mégard, F. 1979. Early Tertiary “Incaic” tectonism, uplift, and volcanic activity, Andes of central Peru. *Geological Society of America Bulletin*, **90,** 903–907.

Palacios, C., Rouxel, O., Reich, M., Cameron, E. M., Leybourne, M. I. 2011. Pleistocene recycling of copper at a porphyry system, Atacama Desert, Chile: Cu isotope evidence. *Mineralium Deposita*, **46**, 1-7.

Perelló, J. 2004. Discovery and geology of the Esperanza porphyry copper-gold deposit, Antofagasta Region, northern Chile. *Andean Metallogeny: New Discoveries, Concepts, and Updates*, 167–186.

Perelló, J. 2010. Wealth creation through exploration in a mature terrain: The case history of the Centinela district, northern Chile porphyry copper belt. *The Chellenge of Finding*

New Mineral Resources: Global Metallogeny, Innovative Exploration, and New Discoveries, 229–252.

Piquer, J., Hollings, P., Rivera, O., Cooke, D. R., Baker, M., and Testa, F. 2017. Along-strike segmentation of the Abanico Basin, central Chile: New chronological, geochemical and structural constraints. *Lithos*, **268**, 174–197.

Quang, C. X., Clark, A. H., Lee, J. K., and Hawkes, N. 2005. Response of supergene processes to episodic Cenozoic uplift, pediment erosion, and ignimbrite eruption in the porphyry copper province of southern Peru. *Economic Geology*, **100**, 87–114.

Reich, M., Palacios, C., Vargas, G., Luo, S., Cameron, E. M., Leybourne, M. I., Parada, M. A., Zúñiga, A. You, C.-F. 2009. Supergene enrichment of copper deposits since the onset of modern hyperaridity in the Atacama Desert, Chile. *Mineralium Deposita*, **44**, 497-504.

Reich, M., and Vasconcelos, P. M. 2015. Geological and economic significance of supergene metal deposits. *Elements*, **11**, 305–310.

Richards, J. P. 2011. Magmatic to hydrothermal metal fluxes in convergent and collided margins. *Ore Geology Reviews*, **40**, 1–26.

Riquelme, R., Hérail, G., Martinod, J., Charrier, R., and Darrozes, J. 2007. Late Cenozoic geomorphologic signal of Andean forearc deformation and tilting associated with the uplift and climate changes of the Southern Atacama Desert (26 S–28 S). *Geomorphology*, **86**, 283–306.

Riquelme, R., Tapia, M., Campos, E., Mpodozis, C., Carretier, S., Gonzalez, R., Muñoz, S., Fernandez-Mort, A., Sanchez C., and Marquardt, C. Sedimentological constrains on unroofing history and geomorphologic conditions allowing supergene and exotic-Cu mineralization from porphyry coppers: the Middle Eocene to Middle Miocene Centinela Basin, Atacama Desert. *Basin Research*, Accepted

Seedorff, E., Dilles, J. H., Proffett, J. M., Einaudi, M. T., Zurcher, L., Stavast, W. J. A., Johnson, D.A., Barton, M. D. 2005. Porphyry deposits: Characteristics and origin of hypogene features. In: *Economic Geology 100th Anniversary Volume* (J.W. Hedenquist, J.F.H. Thompson, R.J. Goldfarb, and J.P. Richards). *Society of Economic Geologists, Inc.*, 251–298.

Segerstrom, K. 1963. Matureland of northern Chile and its relationship to ore deposits. *Geological Society of America Bulletin*, *74*(4), 513–518.

Sillitoe, R. H., and McKee, E. H. 1996. Age of supergene oxidation and enrichment in the Chilean porphyry copper province. *Economic Geology*, **91**, 164–179.

Sillitoe, R.H., 2005. Supergene oxidized and enriched porphyry copper and related deposits. In: *Economic Geology 100th Anniversary Volume* (J.W. Hedenquist, J.F.H. Thompson, R.J. Goldfarb, and J.P. Richards). *Society of Economic Geologists, Inc.*, 723–768.

Sillitoe, R. H., and Perelló, J. 2005. Andean copper province: Tectonomagmatic settings, deposit types, metallogeny, exploration, and discovery. In: *Economic Geology 100th Anniversary Volume* (J.W. Hedenquist, J.F.H. Thompson, R.J. Goldfarb, and J.P. Richards). *Society of Economic Geologists, Inc.*, 845–890.

Steinmann, G., Stappenbeck, R., Sieberg, A. H., and Lissón, C. I. 1929. *Geologie von Perú: mit 9 Tafeln, 271 Textabbildungen und Geologischer Karte 1: 3000000*. Carl Winters Universitätsbuchhandlung.

Tomlinson, A. J., and Blanco, N. 1997. Structural evolution and displacement history of the West Fault System, Precordillera, Chile: Part 2, postmineral history. In *Congreso Geológico Chileno* (Vol. 8, p. 1878–1882).

Vasconcelos, P. M., Reich, M., and Shuster, D. L. 2015. The paleoclimatic signatures of supergene metal deposits. *Elements*, **11**, 317–322.

Vasconcelos, P.-M. 1999. K-Ar and 40Ar/39Ar geochronology of weathering processes. *Annual Review of Earth and Planetary Sciences*, **27**, 183–229.

Wilkinson, J. J. 2013. Triggers for the formation of porphyry ore deposits in magmatic arcs. *Nature Geoscience*, **6**, 917.

Witt, C., Rangin, C., Andreani, L., Olaez, N., and Martinez, J. 2012. The transpressive left-lateral Sierra Madre de Chiapas and its buried front in the Tabasco plain (southern Mexico). *Journal of the Geological Society*, **169**, 143–155.

Wu, L., Monié, P., Wang, F., Lin, W., Ji, W., Bonno, M., Münche, P., Wang, Q. 2016. Cenozoic exhumation history of Sulu terrane: Implications from (U–Th)/He thermochrology. *Tectonophysics*, **672**, 1–15.

DATA REPOSITORY

Table A1. $^{39}Ar/^{40}Ar$ and K/Ar supergene and exotic ages of the Centinela District.

Table A2. Zircon U–Pb data.

Figure A1. U–Pb concordia spots for samples DC12-03, DC12-06, DC12-08 and DC12-10.

Table A3. Apatite fission track data.

Table A4. Apatite (U–Th)/He data.

Figure A2. HeFty modelling.

FIGURE CAPTIONS

Figure 1. Schematic evolution of the denudation rate through time in response to a period of surface uplift. WT: water table (dashed line); SCM: supergene copper mineralization (blue layer).

Figure 2. A. Location of the studied area in the South American continent. B. Morpho-structural map of northern Chile (CC: Coastal Cordillera, CV: Central Valley; PC:

Precordillera; AS: Atacama Salar; AP: Altiplano after Jordan et al., 1983). Red square marks the location of the Centinela District. C. Detailed Centinela District map after Mpodozis and Cornejo (2012), showing sample locations and ages ($^{40}Ar/^{39}Ar$ – K/Ar are from Sillitoe and Mckee, 1996; Perello et al., 2010, and Riquelme et al., accepted).*Zircon U–Pb ages from Antofagasta Mineral SA, personal communication.

Figure 3. Temperature vs. time paths, modelled from HeFTy (Ketcham, 2005), U–Pb dating (from this study and geological map) and $^{40}Ar/^{39}Ar$ and K/Ar supergene ages (see tables in the supplementary data) of six samples. The envelopes represent the possible "good paths" obtained for 10000 Monte Carlo simulations for each sample. We superimposed the envelopes for the six samples providing AFT and AHe ages, and added mean best-fit paths for the Palaeocene and Eocene sample groups (three samples in each).

Table 1. Global data set. Altitude, sample location, rock type and zircon U–Pb, AFT and AHe age results; track measurement details (number measured, Dpar = etch pit width). Asterisks indicate unpublished ages from Antofagasta Minerals.

Name	**Altitude (m)**	**Latitude**	**Longitude**	**Rock type**	**Age U–Pb (Ma)**	**Age FT (Ma)**	**Track lengths *N* tracks**	**Dpar (StD)**	**Age He (Ma)**
DC12-01	2323	23°14’23”	69°11’52”	Dacitic	42.7* ± 0.7	40.6 ± 3.3	14.00 ± 0.11 100	2.7 ± 0.37	29.9 ± 2.1
DC12-03	2226	22°56’44”	69°01’32”	Dacitic, mineralized	40.5 ± 1.1	40.0 ± 2.7	14.99 ± 0.15 62	2.9 ± 1.30	31.2 ± 7.5
DC12-06	2955	23°02’34”	68°57’41”	Dacitic	40.3 ± 1.3	37.1 ± 5.2	14.84 ± 0.15 59	2.6 ± 1.56	29.1 ± 3.4
DC12-08	2149	23°01’22”	69°09’40”	Granodiorite	64.9 ± 1.2	41.4 ± 3.1	13.98 ± 0.30 99	1.8 ± 0.86	52.4 ± 3.7
DC12-09	2012	23°01’56”	69°11’26”	Granodiorite	-	46.1 ± 4.8	13.96 ± 0.30 41	3.9 ± 0.90	22.4 ± 3.8
DC12-10	2082	23°07’31”	69°10’37”	Granodiorite	64.4 ± 1.4	-	-	-	45.0 ± 3.1
DC12-12	2611	23°04’23”	69°10’26”	Granodiorite	-	-	-	-	35.8 ± 2.7
DC12-13	2847	23°08’60”	69°06’03”	Granodiorite	-	-	-	-	43.1 ± 7.0
DC12-14	2375	23°07’22”	69°06’26”	Dacitic	49.3* ± 1.3	-	-	-	16.2 ± 3.3
DC12-15	2183	23°09’50”	69°08’27”	Dacitic	-	42.5 ± 3.4	13.96 ± 0.30 58	2.3 ± 0.26	36.9 ± 2.6

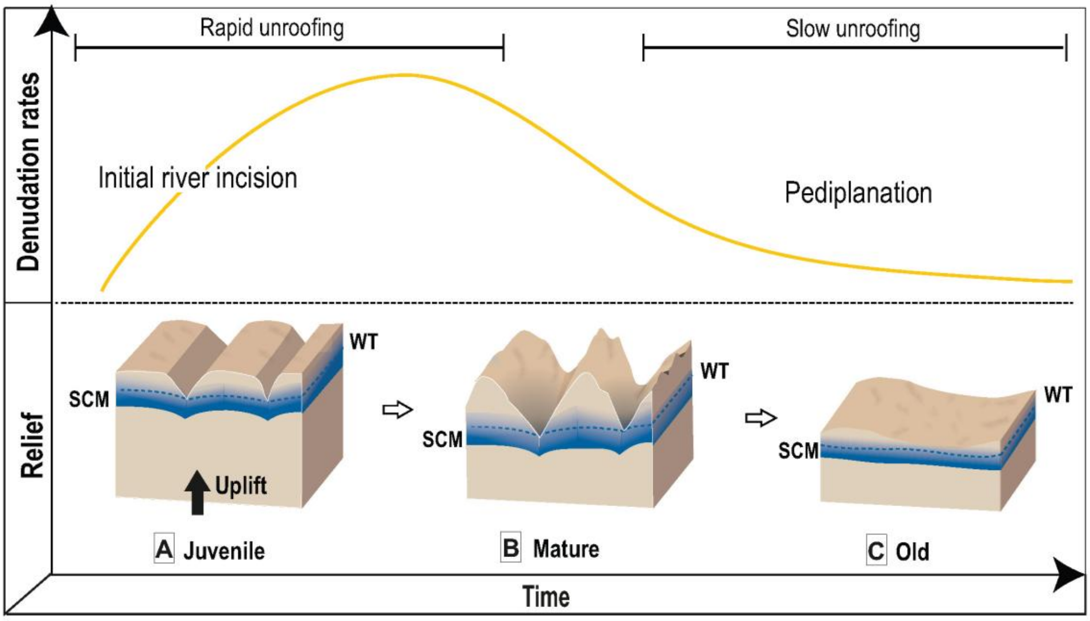

Rapid unroofing
Slow unroofing
Denudation rates
Initial river incision
Pediplanation
Relief
SCM
WT
Uplift
A Juvenile
B Mature
C Old
Time

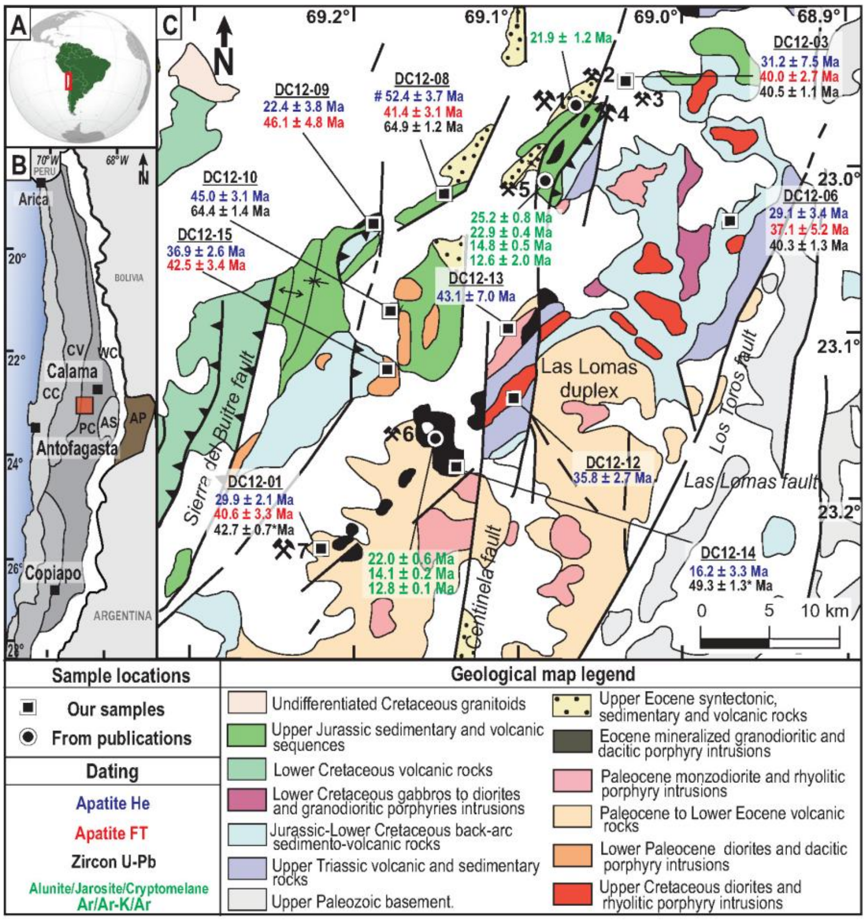

A
B
C
69.2°
69.1°
69.0°
68.9°
23.0°
23.1°
23.2°
N
Arica
PERU
BOLIVIA
70°W
68°W
20°
22°
24°
26°
28°
CV
WC
Calama
CC
PC
AS
AP
Antofagasta
Copiapo
ARGENTINA
DC12-09
22.4 ± 3.8 Ma
46.1 ± 4.8 Ma
DC12-08
52.4 ± 3.7 Ma
41.4 ± 3.1 Ma
64.9 ± 1.2 Ma
21.9 ± 1.2 Ma
DC12-03
31.2 ± 7.5 Ma
40.0 ± 2.7 Ma
40.5 ± 1.1 Ma
DC12-10
45.0 ± 3.1 Ma
64.4 ± 1.4 Ma
DC12-15
36.9 ± 2.6 Ma
42.5 ± 3.4 Ma
25.2 ± 0.8 Ma
22.9 ± 0.4 Ma
14.8 ± 0.5 Ma
12.6 ± 2.0 Ma
DC12-06
29.1 ± 3.4 Ma
37.1 ± 5.2 Ma
40.3 ± 1.3 Ma
DC12-13
43.1 ± 7.0 Ma
Las Lomas duplex
Sierra del Buitre fault
Los Toros fault
DC12-12
35.8 ± 2.7 Ma
Las Lomas fault
DC12-01
29.9 ± 2.1 Ma
40.6 ± 3.3 Ma
42.7 ± 0.7*Ma
22.0 ± 0.6 Ma
14.1 ± 0.2 Ma
12.8 ± 0.1 Ma
Centinela fault
DC12-14
16.2 ± 3.3 Ma
49.3 ± 1.3* Ma
0
5
10 km
1
2
3
4
5
6
7
Sample locations
Our samples
From publications
Dating
Apatite He
Apatite FT
Zircon U-Pb
Alunite/Jarosite/Cryptomelane Ar/Ar-K/Ar
Geological map legend
Undifferentiated Cretaceous granitoids
Upper Jurassic sedimentary and volcanic sequences
Lower Cretaceous volcanic rocks
Lower Cretaceous gabbros to diorites and granodioritic porphyries intrusions
Jurassic-Lower Cretaceous back-arc sedimento-volcanic rocks
Upper Triassic volcanic and sedimentary rocks
Upper Paleozoic basement.
Upper Eocene syntectonic, sedimentary and volcanic rocks
Eocene mineralized granodioritic and dacitic porphyry intrusions
Paleocene monzodiorite and rhyolitic porphyry intrusions
Paleocene to Lower Eocene volcanic rocks
Lower Paleocene diorites and dacitic porphyry intrusions
Upper Cretaceous diorites and rhyolitic porphyry intrusions

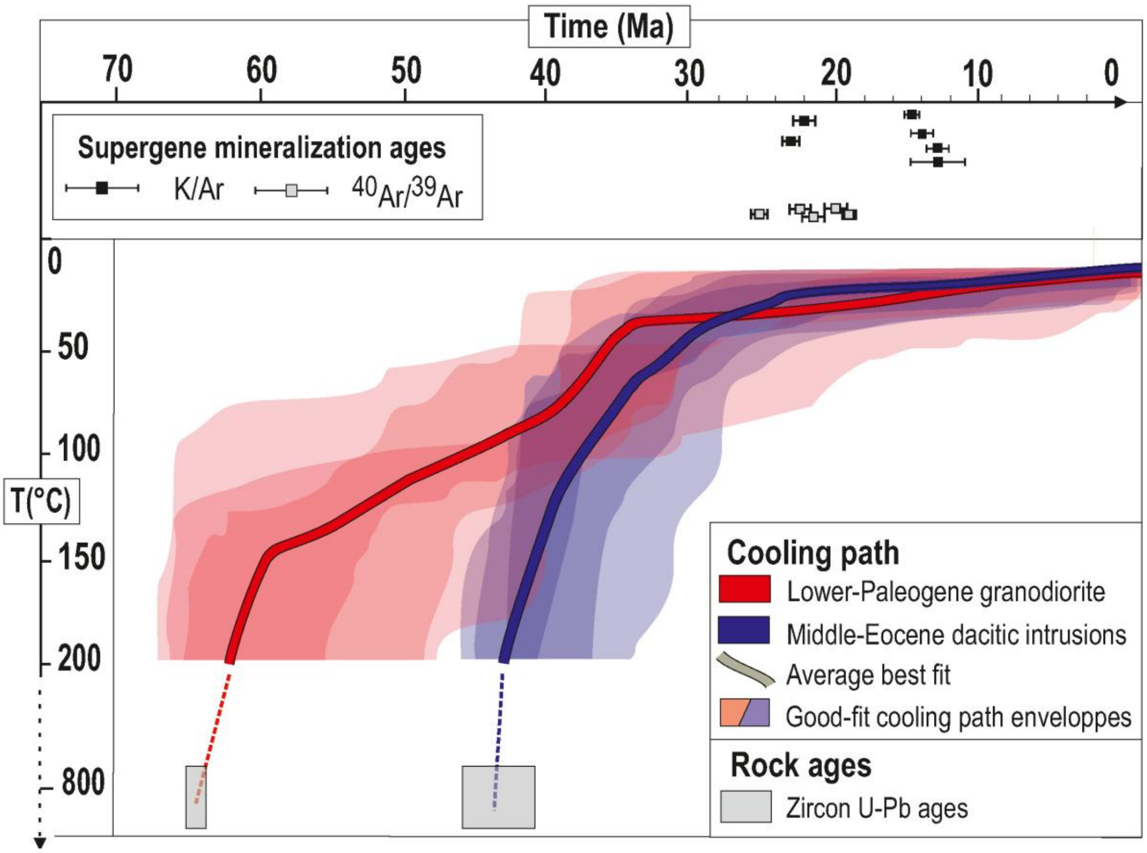
Time (Ma)
70
60
50
40
30
20
10
0
Supergene mineralization ages
K/Ar
$^{40}Ar/^{39}Ar$
T(°C)
0
50
100
150
200
800
Cooling path
Lower-Paleogene granodiorite
Middle-Eocene dacitic intrusions
Average best fit
Good-fit cooling path enveloppes
Rock ages
Zircon U-Pb ages